ACS Energy LETTERS

http://pubs.acs.org/journal/aelccp

LETTER

Molecular Design of Fused-Ring Phenazine Derivatives for Long-Cycling Alkaline Redox Flow Batteries

Caixing Wang, Xiang Li, Bo Yu, Yanrong Wang, Zhen Yang, Huaizhu Wang, Huinan Lin, Jing Ma, Guigen Li, and Zhong Jin*

Cite This: *ACS Energy Lett.* 2020, 5, 411−417

Read Online

ACCESS | Metrics & More | Article Recommendations | Supporting Information

ABSTRACT: The utilization of redox-active organic species in aqueous redox flow batteries holds great promise for large-scale and sustainable energy storage. Herein, we report the low-temperature green synthesis of three different phenazine derivatives and investigate their performances in alkaline organic redox flow batteries. Electrochemical characterizations reveal that the ortho-substituents of the hydroxyl groups in phenazine derivatives have significant influences on the battery performances. By introducing an additional phenyl group adjacent to the hydroxyl group in the phenazine motif and a carboxyl group with strong solubilizing effect, the redox flow battery based on fused-ring benzo[*a*]hydroxyphenazine-7/8-carboxylic acid with 1.0 M electron concentration exhibits greatly improved capacity retention rate of 99.986% cycle^{-1} (99.92% day^{-1}) and stable average energy efficiency of ∼80% for over 1300 cycles. Moreover, a combinatorial library of hydroxyphenazine derivatives with varying substituent groups was built, and their redox properties were simulated to guide further molecular structure design of phenazine-derived electroactive compounds.

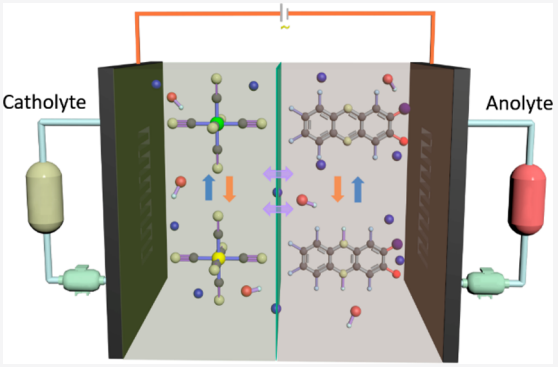

The exploitation of renewable and distributed energy sources, such as solar and wind power, has made significant progress in the past decades,[1−5] but their intermittency and volatility seriously limit the application in grid-connected power systems.[6,7] It is essential to develop large-scale energy storage systems that can rapidly respond and buffer the electricity flux from renewable energy sources to the grid. Redox flow batteries (RFBs) can conveniently store substantial electrochemical energy in the electroactive materials dissolved in an electrolyte and kept in reservoir tanks, which brings the advantages of high scalability and variable modular design with independent control on energy and power.[8−10] Therefore, RFBs represent a promising grid-scale energy storage technology for peak-shaving and valley-filling and have attracted rising interest from academia, industry, and public utilities. For now, most of the extensively studied aqueous RFBs (ARFBs), such as all-vanadium, iron/chromium, and zinc/bromine RFB systems,[11−13] are based on inorganic redox couples, especially metal-based electroactive species. Due to the restriction of the inherent characteristics of inorganic redox species, the widespread adoption of conventional ARFBs is hampered by the relatively low Coulombic efficiency, high system cost, environmental issues, and limited resources.[14,15] To overcome these obstacles toward sustainable applications, the design of high-performance ARFBs based on low-cost and environmentally benign electroactive species is of great importance.

In recent years, the design and utilization of redox-active organic molecules as active species in ARFBs have aroused rising attention,[16−19] owing to the low synthesis costs, rich structural diversity, and tunable multielectron redox properties enabled by functional group modification.[20−25] However, organic-based electroactive materials may exhibit low solubility and poor chemical stability in aqueous solution, resulting in low energy density and shortened cycling life. The degradation mechanism of organic molecules in nonaqueous system has been widely studied for many years,[26−30] while the capacity fade mechanism of organic redox-active species in aqueous systems has attracted rising attention over the last 5 years.[31−33] To date, the redox reversibility of water-soluble organic

Received: December 9, 2019
Accepted: January 6, 2020
Published: January 6, 2020

https://dx.doi.org/10.1021/acsenergylett.9b02676
ACS Energy Lett. 2020, 5, 411−417

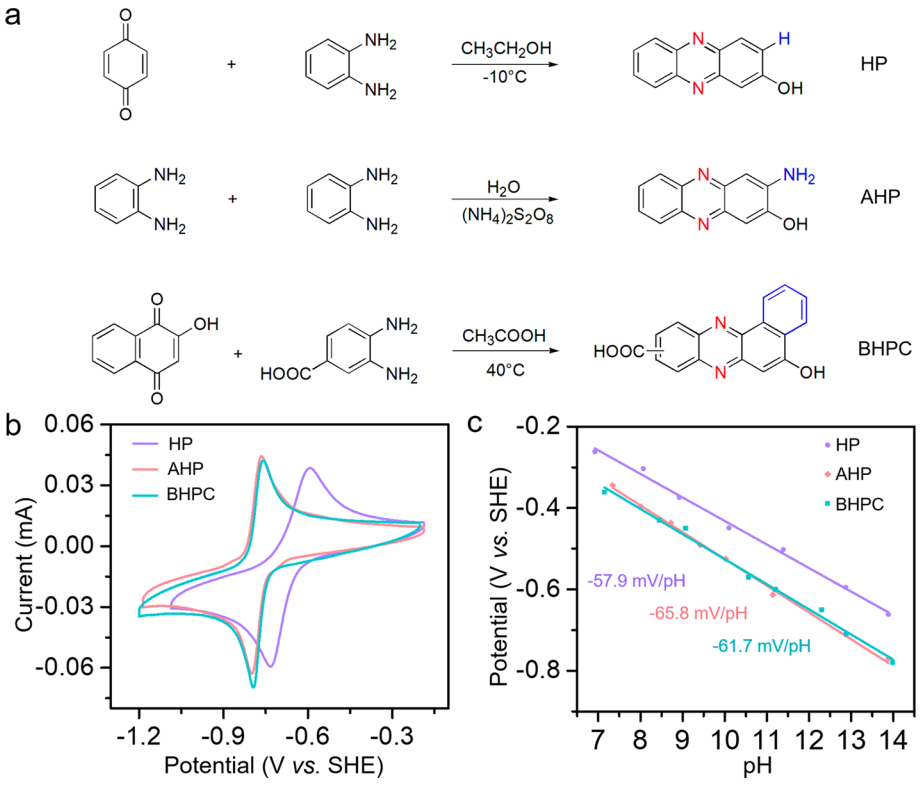

Figure 1. Synthesis routes and redox properties of hydroxyphenazine derivatives. (a) Synthesis routes of HP, AHP, and BHPC molecules. (b) CV curves of HP, AHP, and BHPC molecules (with 2 mM concentration) measured by a 3 mm glassy carbon electrode in 1.0 M KOH solution at a scanning rate of 100 mV s^{-1}. (c) Pourbaix diagrams of HP, AHP, and BHPC molecules.

molecules has been successfully extended to varying degrees.[34−37] Phenazine and its derivatives have been widely used as broad-spectrum antibiotics.[38] It has been found that phenazine shows reversible redox properties in water−DMF mixtures,[39,40] but its insolubility in water hinders the application in ARFBs. Through the grafting of triethylene glycol (TEG) linkers or sulfonate groups, the solubility of phenazine derivatives can be increased to different extents.[41,42] Meanwhile, the effects of different functional groups of phenazine derivatives on the aqueous solubility, electrochemical redox properties, and cycling stability are waiting to be further explored.

Herein, we investigate and compare the performances of three different low-potential phenazine derivatives, including 2-hydroxyphenazine (HP), 2-amino-3-hydroxyphenazine (AHP), and benzo[*a*]hydroxyphenazine-7/8-carboxylic acid (BHPC) as the active species in the anolyte of alkaline ARFBs, and coupled them with low-cost ferricyanide catholyte.[43,44] We find that the substituted groups adjacent to the hydroxyl group in hydroxyphenazine have dramatic influences on the redox potential, solubility, and cycling stability. Briefly, HP with 2-H shows a potential of −0.67 V vs a standard hydrogen electrode (SHE) and a high solubility of 1.8 M, but the cycling stability in ARFBs is not satisfying. By turning the 2-H to an NH_2 group, the redox potentials of AHP are negatively shifted by over 100 mV, and the redox stability is greatly improved. Inspired by these results, we further propose the design of a new molecule BHPC with an adjacent large, noncharged phenyl block group (2-position) and an additional carboxyl group (on the 7/8-position to further enhance its solubility). The ARFB based on 0.5 M BHPC anolyte and excess ferrocyanide catholyte exhibits a low fade rate of 0.08% day^{-1} for over 1300 cycles and an output power density of 0.43 W cm^{-2}, which is competitive among the state-of-the-art organic ARFBs.[16−25,32−37,45] The redox properties of these hydroxyphenazine derivatives were evaluated by Pourbaix diagrams, pH-dependent UV−vis spectra and time-dependent density functional theory (TDDFT) simulations,[46−48] confirming the non-negligible resonance effect of functional groups and intramolecular hydrogen bonds. Moreover, we built a combinatorial library of numerous phenazine derivatives, and their redox potentials were computed and predicted based on the phenol−ketone isomerization principle, which could provide insightful guidance to further development of alkaline ARFBs with high voltage and long cycling life.

The three designated phenazine derivatives were successfully synthesized on a large scale from low-cost quinone and diaminobenzene precursors in nontoxic solvents at different temperatures (Figure 1a), as detailed in the Methods section of the Supporting Information. Different from the traditional Wohl−Aue reaction normally used for the synthesis of phenazine,[41] we utilized a cyclization reaction between aromatic amine and quinone. This synthesis method has the advantages of cheaper precursors, less reaction steps, milder conditions, and higher yields and represents a more economical and greener synthesis route. Briefly, HP was synthesized in ethanol solvent at a low temperature (−10 °C) with a yield of 70%. AHP was obtained from a dimerization and hydroxylation process of an *o*-diaminobenzene precursor at room temperature with a yield of >80%. BHPC was easily prepared by mixing lawsone and 3,4-diaminobenzoic acid in acetic acid at 40 °C with a high yield (>93%) and no byproduct. The synthesis of these three molecules was confirmed by nuclear magnetic resonance (NMR) and liquid

https://dx.doi.org/10.1021/acsenergylett.9b02676
ACS Energy Lett. 2020, 5, 411−417

chromatography mass spectrometry (LC-MS) (Figures S1–S8). Compared to other reported redox-active molecules, the costs for preparing these hydroxyphenazine derivatives are very low (Table S1).

The electrochemical properties of these phenazine derivatives were analyzed by cyclic voltammetry (CV) in 1.0 M KOH aqueous solution (Figure 1b). HP exhibits a formal potential of −0.67 V (vs SHE) with a peak separation of 140 mV, while AHP and BHPC show a similar potential of −0.78 V with a lower peak separation of 34 mV, which might due to the intermolecular hydrogen bonds and larger conjugated structures. When paired with ferrocyanide catholyte, the alkaline ARFBs based on these phenazine derivative anolytes can exhibit different open-circuit voltages (OCVs) ranging from 1.16 to 1.27 V. To explore the proton and electron transfer behavior during the redox processes, the CV curves of these molecules at different pH values were also measured (Figure S9), which exhibited similar shapes at neutral and alkaline conditions. The Pourbaix diagrams calculated from the CV curves measured at different pH values are shown in Figure 1c; the relevant slopes for HP, AHP, and BHPC are estimated to be −57.9, −65.8, and −61 mV pH^{-1} (compared to the theoretical value of −59.2 mV pH^{-1}), which is in accord with a two-electron/two proton process. This result indicates that the higher pH value is helpful for elevating the open-circuit voltage and the output power density of ARFBs based on these phenazine derivatives.

To investigate the pH-dependent structural transformation behaviors of these phenazine derivatives in aqueous solution, UV–vis spectra were measured at different pH values,[39] as shown in Figure 2. Moreover, the TDDFT-simulated light absorption lines of these molecules were obtained by calculating the energy levels of the HOMO (highest occupied molecular orbital) and LUMO (lowest occupied molecular orbital),[47,48] as shown in the insets of Figure 2b,d,f. The HP molecule could be deprotonated at pH around 7.6 (Figure S10a). According to the TDDFT simulation result, the absorbance peaks of HP observed at $\lambda_{471\ nm}$ and $\lambda_{374\ nm}$ are predicted to be the electronic transition of HOMO−1 and HOMO−2 to LUMO, respectively (Figure 2a,b). AHP shows a slightly higher pK_a value of 7.8 compared to HP (Figure S10b) but only has one absorbance peak in the visible band. As the pH increases, this peak blue shifts from 471 nm (pH 7) to 422 nm (pH 14), corresponding to the transition from HOMO−1 to LUMO (Figure 2c,d). BHPC possesses two pK_a values of around 5.0 and 7.6 (Figure 2e,f), which can be ascribed to the dissociation of carboxyl and phenol groups, respectively (Figure S10c). With one more conjugated aromatic ring, the absorption peaks of BHPC exhibit a strong red shift. As the pH value increases from 7 to 14, the absorbance peak of BHPC in the visible band is blue-shifted from $\lambda_{502\ nm}$ to $\lambda_{490\ nm}$, which matches well with the transition of HOMO to LUMO (with a simulated spectral line at $\lambda_{489\ nm}$). The simulated light absorption spectral lines of these molecules are consistent with the experimental spectra, confirming their structural conformation at different pH values. The predicted potentials of the three phenazine derivatives were evaluated based on the Gibbs free energy differences between the oxidized and reduced forms and converted to the values at pH 14 on the Pourbaix diagrams in Figure 1d. The calculation average errors compared with the measured values are less than 15 mV (Figure 2g), which is much lower than the previously reported hydroxyphenazines

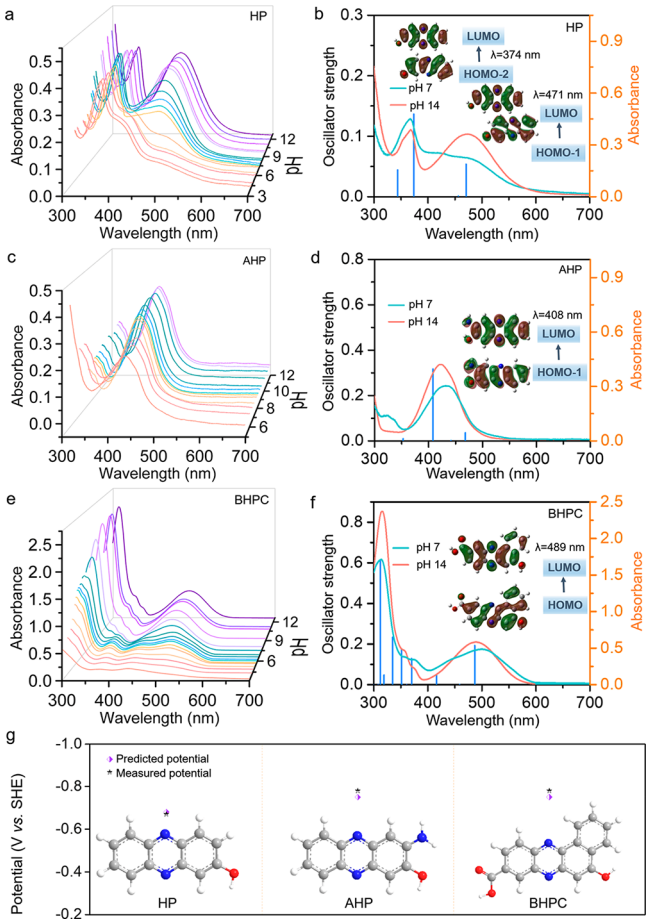

Figure 2. UV–vis spectra of (a) HP, (c) AHP, and (e) BHPC at different pH values. TDDFT-simulated light absorption lines at pH 7 and the measured UV–vis spectra at pH 7 and 14 of (b) HP, (d) AHP, and (f) BHPC. The insets in (b,d,f) represent the relevant transition orbitals in the visible band. (g) Comparison between the predicted and measured potentials of three phenazine derivatives at pH 14.

(~300 mV).[42] According to the absorbance curves (Figure S11), the solubilities of HP, AHP, and BHPC in KOH solution are measured to be 1.70, 0.43, and 1.55 M, respectively (Table 1). In comparison, the relevant values are measured to be 0.44, 0.57, and 16.0 mM in neutral buffer solution (Figure S12). The results ensure the good solubilizing effect of the carboxyl group in alkaline solution. The reason for the low solubility of AHP could be ascribed to the intramolecular hydrogen bonds between the hydroxyl anion and the adjacent amino group, and the reason for the high solubility of BHPC in alkaline solution shall be mainly attributed to the solubilization effect of the carboxyl group (Figure S12c), which has also been observed in previous literature.[18,45]

To understand the redox reaction kinetics of phenazine derivatives, the diffusion coefficients (D) and rate constants (k_0) were investigated by linear sweep voltammetry (LSV),[49] as shown in Figures S13–S15. All of the reduction limiting diffusion current plateaus were gradually stabilized by the cathodic polarization from the equilibrium potential to a lower potential at a scanning rate of 25 mV s^{-1}. Calculated from the linear fitting relationship between the limiting diffusion currents and the root of the rotation rates, the diffusion coefficients of HP, AHP, and BHPC were calculated to be 3.79

https://dx.doi.org/10.1021/acsenergylett.9b02676
ACS Energy Lett. 2020, 5, 411–417

Table 1. Summary of the Physiochemical Properties of As-Prepared Phenazine Derivatives

compound	solubility (M)	E (vs SHE)	pK_a	k_0 (cm s^{-1})	D (cm s^{-2})
HP	1.70	−0.67	7.6	1.42×10^{-3}	3.79×10^{-6}
AHP	0.43	−0.78	7.8	1.63×10^{-3}	2.85×10^{-6}
BHPC	1.55	−0.78	5.0, 7.6	1.55×10^{-3}	3.52×10^{-6}

$\times 10^{-6}$, 2.85×10^{-6}, and 3.52×10^{-6} cm^2 s^{-1}, respectively. The Koutecký−Levich plots were fitted to the Butler−Volmer equation, and the electron-transfer rate constants of HP, AHP, and BHPC were calculated to be 1.42×10^{-3}, 1.63×10^{-3}, and 1.55×10^{-3} cm s^{-1} according to the Tafel plots, respectively. The physiochemical parameters of these molecules in 1.0 M KOH are also listed in Table 1. These results verify that the redox rate and reversibility of organic species can be conveniently adjusted by modifying the functional groups, which is distinct from simple metal ions.

The working performances of ARFBs coupled by different phenazine derivative anolytes and excess ferrocyanide catholytes at low concentrations were first investigated, as shown in Figure 3. The $K_4Fe(CN)_6$||HP ARFB exhibits an OCV of 1.16 V and delivers initial discharge capacities of 3.65 and 3.25 Ah L^{-1} at 50 and 100 mA cm^{-2}, respectively (Figures 3a and S15). A cycling test shows that the capacity of $K_4Fe(CN)_6$||HP ARFB quickly fades from 3.25 to 1.23 Ah L^{-1} after 100 cycles, although the Coulombic efficiency maintains at ∼100% (Figure 3b). After the cycling test, some precipitation appears

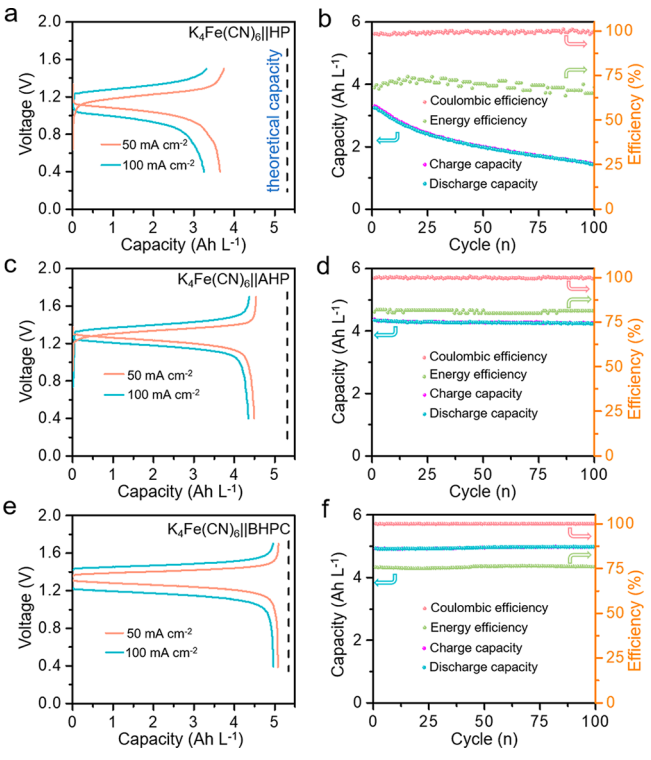

Figure 3. Performances of ferricyanide/phenazine derivative ARFBs at low concentrations. The electrolytes in the cell are comprised of 15 mL of 0.2 M ferricyanide catholyte and 10 mL of 0.1 M phenazine derivative anolyte. (a,c,e) Charge−discharge curves of the ARFBs based on (a) HP, (c) AHP, and (e) BHPC anolytes at current densities of 50 and 100 mA cm^{-2}. The black dashed lines indicate the theoretical specific capacities. (b,d,f) Cycling performances of the ARFBs based on (b) HP, (d) AHP, and (f) BHPC anolytes at a current density of 100 mA cm^{-2}.

in the HP anolyte, and a new redox peak pair is presented in the CV curve of the cycled HP anolyte (Figure S17a). The UV−vis spectrum shows a different peak shape at pH 14 (Figure S17b), and a peak at m/z 389.05 is also found in the LC-MS spectrum, indicating a dimerization process between its reduction state and oxidation state during cycling, as illustrated in Figure S18. The $K_4Fe(CN)_6$||AHP ARFB shows an OCV of 1.27 V (Figure 3c) and delivers initial discharge capacities of 4.39 and 4.35 Ah L^{-1} at 50 and 100 mA cm^{-2}, respectively, with a capacity retention of >99% and an average energy efficiency of 80% after 100 cycles (Figure 3d), which is very superior to those of $K_4Fe(CN)_6$||HP ARFB. In comparison, the $K_4Fe(CN)_6$||BHPC ARFB shows a high OCV of 1.28 V and initial discharge capacities of 5.12 and 4.98 Ah L^{-1} at 50 and 100 mA cm^{-2}, respectively (Figure 3e), with a high capacity retention of >99% and an average energy efficiency of 77% after 100 cycles (Figure 3f). Different from the HP anolyte, the AHP and BHPC anolytes show no obvious change after cycling, as measured by CV and UV−vis spectroscopy (Figure S17c−f), indicating that no dimerization process has occurred.

Considering the instability of HP in its reduction state and the low solubility of AHP, BHPC is regarded as the most promising candidate among these three molecules. We tested the performances of $K_4Fe(CN)_6$||BHPC ARFB at a high concentration of 0.5 M BHPC anolyte in a 1.0 M KOH solution at a current density of 100 mA cm^{-2} (Figure 4). Benefiting from the electron-donating phenyl group, the $K_4Fe(CN)_6$||BHPC ARFB exhibited a maximum output power density of 0.43 W cm^{-2} at ∼100% SOC (Figure 4a). Figure 4b shows the charge−discharge curves at the 20th, 600th, and 1300th cycles. The charge and discharge voltage plateaus were maintained well during the whole cycling process (with merely a 40 mV voltage drop), which is superior to the reported ARFB based on 3,4-diaminobenzenesulfonic acid (DHPS) (with a 150 mV voltage drop after 500 cycles),[42] verifying the importance of molecular engineering. Moreover, we also studied the self-discharge behavior of the $K_4Fe(CN)_6$||BHPC ARFB after 1304 cycles, and the interference of O_2 was fully excluded (Figure 4c,d). The battery was first charged to 1.7 V at 100 mA cm^{-2} (∼100 SOC%) and then rested for 24 h, resulting in a drop of OCV from 1.38 to 1.35 V and a capacity fade from 25.4 Ah L^{-1} (charge capacity) to 25.0 Ah L^{-1} (discharge capacity) in the next discharge step, corresponding to a capacity retention of 98.4% (Figure 4c,d). Notably, the charge and discharge capacity fully recovered to 25.4 Ah L^{-1} at the 1305th cycle. This result proves that BHPC in its reduction state is chemically stable, and the capacity drop of 1.5% after resting for 24 h at 100% SOC is possibly caused by the transformation of catholyte (i.e., from ferricyanide to ferrocyanide) or the chemical degradation of catholyte (the catholyte turns dark yellow but without precipitation after 23 days). The long-term cycling performance of $K_4Fe(CN)_6$||BHPC ARFB is shown in Figure 4e. Because of the initial O_2 residue in the cell, the Coulombic efficiency gradually increased from 93.3 to 99.2% during the initial 20 cycles,

https://dx.doi.org/10.1021/acsenergylett.9b02676
ACS Energy Lett. 2020, 5, 411−417

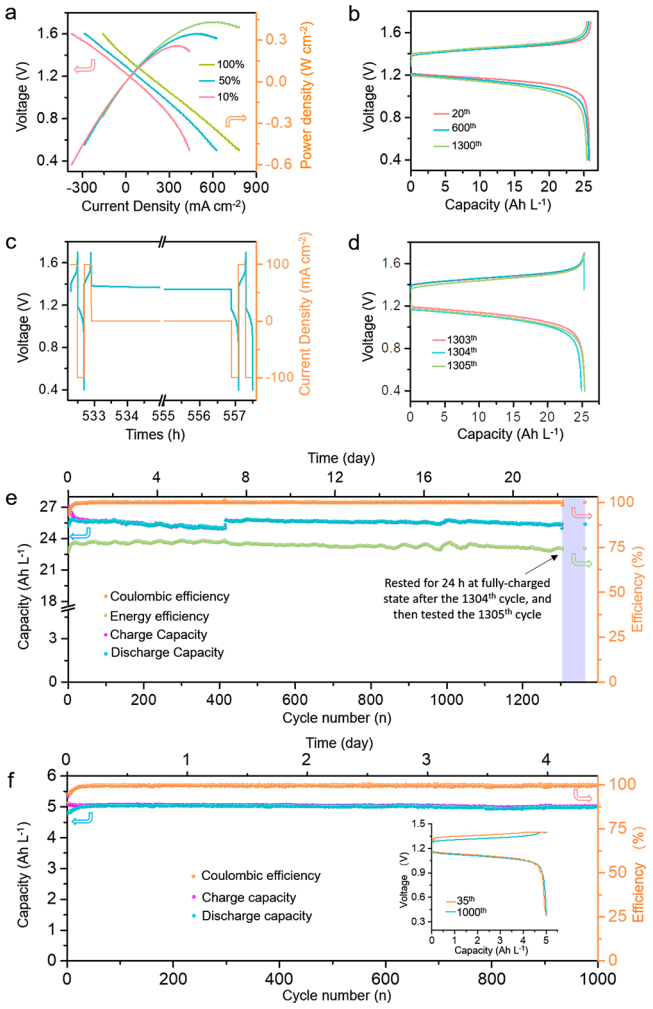

Figure 4. (a) Polarization and power density curves at 10, 50, and 100% SOC, respectively. (b) Charge−discharge curves at different cycles. (c) Self-discharge test at 100% SOC. The battery was rested for 24 h after being fully charged at the 1304th cycle. (d) Corresponding charge−discharge curves from the 1303th to the 1305th cycle. (e) Long-term cycling performance at a current density of 100 mA cm^{-2} for the entire 1305 cycles. The battery was rested for 24 h after being fully charged at the 1304th cycle, and then the 1305th cycle was tested. (f) Galvanostatic−potentiostatic cycling performance at a current density of 100 mA cm^{-2} with the charge potential held at 1.4 V until the current density decreased to 4 mA cm^{-2}.

and the discharge capacity reached the maximum value of 25.9 Ah L^{-1} at the 20th cycle, corresponding to a theoretical capacity utilization rate of 96.7%. After shaking and balancing the anolyte reservoir at the 400th cycle, the $K_4Fe(CN)_6$||BHPC ARFB thereafter worked stably with an average energy efficiency close to 80%. The discharge capacity decreased from 25.9 to 25.4 Ah L^{-1} after the entire 1305 cycles (558 h or over 23 days), corresponding to a capacity retention of 98% or a temporal fade rate of less than 0.08% day^{-1} (or a total of 2.0% in 23 days), providing another effective way besides the dimerization coupling.[43] Such a remarkable capacity retention should be ascribed to the high electrochemical stability of capacity-limiting BHPC anolyte.

The electrochemical performances of BHPC are compared with those of other previously reported molecules, as shown in Table S2. Among them, the ARFB based on DHPS demonstrated the highest OCV of 1.35 V and a relatively high energy density of 10.2 Wh L^{-1} derived from the superior anolyte concentration (1.4 M).[42] However, the ARFB based on DHPS delivered a relatively fast capacity fade rate of ∼0.69% day^{-1} (a total of 9.75% in 14 days), which could possibly be ascribed to the decomposition of catholyte and the membrane insertion of anolyte.[42] In this work, the self-discharge test of $K_4Fe(CN)_6$||BHPC ARFB shows a remarkable capacity retention of 98.4% after resting for 24 h (Figure 4c), and the capacity can be 100% recovered in the following cycles (Figure 4d), confirming the high chemical stability of BHPC in its reduction state. Furthermore, we performed a galvanostatic−potentiostatic cycling test using 0.1 M BHPC anolyte with the charge potential held at 1.4 V until the current density decreased to 4 mA cm^{-2} to eliminate the membrane resistance effect. As shown in Figure 4f, the discharge capacity was only faded from 5.014 to 5.006 Ah L^{-1} for over 1000 cycles (in 4.23 days), corresponding to a fade rate of ∼0.04% day^{-1}. We suggest that the capacity fade of BHPC-based ARFB could be partially a result of the slight increase of membrane resistance, similar to the galvanostatic polarization test results of other redox-active molecules in previous literature.[18,36] The $K_4Fe(CN)_6$||BHPC ARFB exhibits a low fade rate among the representative alkaline ARFBs (Table S2), indicating the importance of molecular design for improving the long-term cycling stability of organic redox-active species. To evaluate the performances of the BHPC molecule at higher concentration, we also tested a $Na_4Fe(CN)_6$||BHPC cell based on 1.0 M BHPC anolyte with a measured energy density of ∼9.5 Wh L^{-1} (Figure S19), confirming the operation feasibility of high-concentration ARFBs based on BHPC and ferrocyanides enabled by mixed Na^+/K^+ cations.[50,51]

Theoretical simulation and prediction of the redox potentials of organic species are helpful to the research of ARFBs. In this work, we calculated the redox potentials of a series of phenazine derivatives for both phenol and keto forms according to the Gibbs energy changes in a neutral environment and converted them to the values at pH 14 based on the Pourbaix diagrams, as shown in Tables S3 and S4. For some molecules, it is notable that the redox potentials could not be precisely predicted by only simulating the phenol form or keto form because the conjugated form should also be considered. The predicted potentials of multihydroxyl phenazine derivatives in Table S3 indicate that the far-end hydroxyl groups can induce a strong electron-donating effect and lower the redox potentials. Moreover, the effects of other functional groups (Table S4), including $-NH_2$, $-NO_2$, $-CH_3$, −COOH, $-OCH_3$, and −Cl on the redox potentials, were also simply simulated by connecting to the 6′-position-substituted 2,3-dihydroxyphenazine (DHP) derivatives. The results indicate that the functional groups and intramolecular hydrogen bonds would greatly affect the redox potentials. Nevertheless, the actual redox potentials and stability of these molecules in alkaline solution require further validation by real experiments.

In summary, the phenazine derivative anolytes studied in this work show high solubility and tunable OCVs of 1.16−1.27 V when coupled with ferrocyanide catholyte. Especially, benefiting from the electron-donating phenyl group and solubilizing carboxyl group, the ARFB based on BHPC with a concentration of 0.5 M exhibited a theoretical capacity utilization rate of >96%, high energy efficiency of ∼80%, high output power density of 0.43 W cm^{-2}, and high capacity

https://dx.doi.org/10.1021/acsenergylett.9b02676
ACS Energy Lett. 2020, 5, 411−417

retention of ~98% for over 1300 cycles at 100 mA cm^{-2} (corresponding to an ultralow capacity fade rate of <0.08% day^{-1}), indicating its great potential for application in alkaline ARFBs. The synthesis cost comparison of the reported redox molecules for alkaline ARFBs also show that the BHPC molecule derived from low-cost and earth-abundant lawsone is a good candidate for active materials for large-scale energy storage. The effective strategy of functional group modification would enlighten more possible routes to solve the capacity fading issue of redox molecules. The theoretical calculation of redox potentials and isomerization behaviors of proposed organic compounds via the combinatorial molecular library are also helpful to predict their electrochemical performances in ARFBs.

■ ASSOCIATED CONTENT

Supporting Information

The Supporting Information is available free of charge at https://pubs.acs.org/doi/10.1021/acsenergylett.9b02676.

Experimental section and additional figures and tables, including NMR spectra, LC-MS spectra, HR-MS spectra, CV curves, absorbance vs pH values plots, UV−vis curves, images of the saturated solutions, possible molecular structures, RDE tests and associated plots, open-circuit voltage vs state of charge curves, high-concentration battery tests, property and price comparisons of different redox-active molecules, performance comparison of high-concentration alkaline organic redox flow batteries, and DFT-calculated properties for combinatorial molecular libraries (PDF)

■ AUTHOR INFORMATION

Corresponding Author

Zhong Jin − *Nanjing University, Nanjing, China, and Shenzhen Research Institute of Nanjing University, Shenzhen, China;* orcid.org/0000-0001-8860-8579; Email: zhongjin@nju.edu.cn

Other Authors

Caixing Wang − *Nanjing University, Nanjing, China*
Xiang Li − *Nanjing University, Nanjing, China*
Bo Yu − *Nanjing University, Nanjing, China*
Yanrong Wang − *Nanjing University, Nanjing, China*
Zhen Yang − *Nanjing University, Nanjing, China*
Huaizhu Wang − *Nanjing University, Nanjing, China*
Huinan Lin − *Nanjing University, Nanjing, China*
Jing Ma − *Nanjing University, Nanjing, China;* orcid.org/0000-0001-5848-9775
Guigen Li − *Nanjing University, Nanjing, China*

Complete contact information is available at: https://pubs.acs.org/10.1021/acsenergylett.9b02676

Notes

The authors declare no competing financial interest.

■ ACKNOWLEDGMENTS

This work is supported by the National Key Research and Development Program of China (2017YFA0208200, 2016YFB0700600, 2015CB659300), Projects of NSFC (21872069, 51761135104, 21672100, 21573108), the Natural Science Foundation of Jiangsu Province for Young Scholars (BK20180008), the High-Level Entrepreneurial and Innovative Talents Program of Jiangsu Province, and the Fundamental Research Funds for the Central Universities (0205-14380188).

■ REFERENCES

(1) Gratzel, M. Solar Energy Conversion by Dye-Sensitized Photovoltaic Cells. *Inorg. Chem.* **2005**, *44*, 6841−6851.
(2) Krebs, F. C. Fabrication and Processing of Polymer Solar Cells: A Review of Printing and Coating Techniques. *Sol. Energy Mater. Sol. Cells* **2009**, *93*, 394−412.
(3) Yun, S.; Qin, Y.; Uhl, A. R.; Vlachopoulos, N.; Yin, M.; Li, D.; Han, X.; Hagfeldt, A. New-Generation Integrated Devices Based on Dye-Sensitized and Perovskite Solar Cells. *Energy Environ. Sci.* **2018**, *11*, 476−526.
(4) Diaz-Gonzalez, F.; Sumper, A.; Gomis-Bellmunt, O.; Villafafila-Robles, R. A Review of Energy Storage Technologies for Wind Power Applications. *Renewable Sustainable Energy Rev.* **2012**, *16*, 2154−2171.
(5) Zhao, H.; Wu, Q.; Hu, S.; Xu, H.; Rasmussen, C. N. Review of Energy Storage System for Wind Power Integration Support. *Appl. Energy* **2015**, *137*, 545−553.
(6) Yang, Z.; Zhang, J.; Kintner-Meyer, M. C.; Lu, X.; Choi, D.; Lemmon, J. P.; Liu, J. Electrochemical Energy Storage for Green Grid. *Chem. Rev.* **2011**, *111*, 3577−3613.
(7) Vazquez, S.; Lukic, S. M.; Galvan, E.; Franquelo, L. G.; Carrasco, J. M. Energy Storage Systems for Transport and Grid Applications. *IEEE Trans. Ind. Electron.* **2010**, *57*, 3881−3895.
(8) Ponce de León, C.; Frías-Ferrer, A.; González-García, J.; Szánto, D. A.; Walsh, F. C. Redox Flow Cells for Energy Conversion. *J. Power Sources* **2006**, *160*, 716−732.
(9) Wang, W.; Luo, Q. T.; Li, B.; Wei, X. L.; Li, L. Y.; Yang, Z. G. Recent Progress in Redox Flow Battery Research and Development. *Adv. Funct. Mater.* **2013**, *23*, 970−986.
(10) Wei, X. L.; Pan, W. X.; Duan, W. T.; Hollas, A.; Yang, Z.; Li, B.; Nie, Z. M.; Liu, J.; Reed, D.; Wang, W.; Sprenkle, V. Materials and Systems for Organic Redox Flow Batteries: Status and Challenges. *ACS Energy Lett.* **2017**, *2*, 2187−2204.
(11) Skyllas-Kazacos, M.; Rychcik, M.; Robins, R. G.; Fane, A. G.; Green, M. A. New All-Vanadium Redox Flow Cell. *J. Electrochem. Soc.* **1986**, *133*, 1057−1058.
(12) Lopezatalaya, M.; Codina, G.; Perez, J. R.; Vazquez, J. L.; Aldaz, A. Optimization Studies on a Fe/Cr Redox Flow Battery. *J. Power Sources* **1992**, *39*, 147−154.
(13) Lim, H. S.; Lackner, A. M.; Knechtli, R. C. Zinc-Bromine Secondary Battery. *J. Electrochem. Soc.* **1977**, *124*, 1154−1157.
(14) Zhao, P.; Zhang, H. M.; Zhou, H. T.; Chen, J.; Gao, S. J.; Yi, B. L. Characteristics and Performance of 10 kW Class All-Vanadium Redox-Flow Battery Stack. *J. Power Sources* **2006**, *162*, 1416−1420.
(15) Pan, F.; Wang, Q. Redox Species of Redox Flow Batteries: A Review. *Molecules* **2015**, *20*, 20499−20517.
(16) Huskinson, B.; Marshak, M. P.; Suh, C.; Er, S.; Gerhardt, M. R.; Galvin, C. J.; Chen, X.; Aspuru-Guzik, A.; Gordon, R. G.; Aziz, M. J. A Metal-Free Organic-Inorganic Aqueous Flow Battery. *Nature* **2014**, *505*, 195−198.
(17) Lin, K.; Chen, Q.; Gerhardt, M. R.; Tong, L.; Kim, S. B.; Eisenach, L.; Valle, A. W.; Hardee, D.; Gordon, R. G.; Aziz, M. J.; Marshak, M. P. Alkaline Quinone Flow Battery. *Science* **2015**, *349*, 1529−1532.
(18) Lin, K. X.; Gomez-Bombarelli, R.; Beh, E. S.; Tong, L. C.; Chen, Q.; Valle, A.; Aspuru-Guzik, A.; Aziz, M. J.; Gordon, R. G. A Redox-Flow Battery with an Alloxazine-Based Organic Electrolyte. *Nature Energy* **2016**, *1*, 16102.
(19) Gerhardt, M. R.; Tong, L. C.; Gomez-Bombarelli, R.; Chen, Q.; Marshak, M. P.; Galvin, C. J.; Aspuru-Guzik, A.; Gordon, R. G.; Aziz, M. J. Anthraquinone Derivatives in Aqueous Flow Batteries. *Adv. Energy Mater.* **2017**, *7*, 1601488.
(20) Yang, Z. J.; Tong, L. C.; Tabor, D. P.; Beh, E. S.; Goulet, M. A.; De Porcellinis, D.; Aspuru-Guzik, A.; Gordon, R. G.; Aziz, M. J.

Alkaline Benzoquinone Aqueous Flow Battery for Large-Scale Storage of Electrical Energy. *Adv. Energy Mater.* **2018**, *8*, 1702056.
(21) Liu, T. B.; Wei, X. L.; Nie, Z. M.; Sprenkle, V.; Wang, W. A Total Organic Aqueous Redox Flow Battery Employing a Low Cost and Sustainable Methyl Viologen Anolyte and 4-Ho-Tempo Catholyte. *Adv. Energy Mater.* **2016**, *6*, 1501449.
(22) Luo, J.; Hu, B.; Debruler, C.; Liu, T. L. A pi-Conjugation Extended Viologen as Novel Two-Electron Storage Anolyte for Total Organic Aqueous Redox Flow Battery. *Angew. Chem., Int. Ed.* **2018**, *57*, 231.
(23) Hoober-Burkhardt, L.; Krishnamoorthy, S.; Yang, B.; Murali, A.; Nirmalchandar, A.; Prakash, G. K. S.; Narayanan, S. R. A New Michael-Reaction-Resistant Benzoquinone for Aqueous Organic Redox Flow Batteries. *J. Electrochem. Soc.* **2017**, *164*, A600−A607.
(24) Hu, B.; DeBruler, C.; Rhodes, Z.; Liu, T. L. Long-Cycling Aqueous Organic Redox Flow Battery (AORFB) Towards Sustainable and Safe Energy Storage. *J. Am. Chem. Soc.* **2017**, *139*, 1207−1214.
(25) Wang, C.; Yang, Z.; Wang, Y.; Zhao, P.; Yan, W.; Zhu, G.; Ma, L.; Yu, B.; Wang, L.; Li, G.; Liu, J.; Jin, Z. High-Performance Alkaline Organic Redox Flow Batteries Based on 2-Hydroxy-3-Carboxy-1,4-Naphthoquinone. *ACS Energy Lett.* **2018**, *3*, 2404−2409.
(26) Kaur, A. P.; Holubowitch, N. E.; Ergun, S.; Elliott, C. F.; Odom, S. A. A Highly Soluble Organic Catholyte for Non-Aqueous Redox Flow Batteries. *Energy Technol-Ger* **2015**, *3*, 476−480.
(27) Sevov, C. S.; Hickey, D. P.; Cook, M. E.; Robinson, S. G.; Barnett, S.; Minteer, S. D.; Sigman, M. S.; Sanford, M. S. Physical Organic Approach to Persistent, Cyclable, Low-Potential Electrolytes for Flow Battery Applications. *J. Am. Chem. Soc.* **2017**, *139*, 2924−2927.
(28) Zhang, J. J.; Yang, Z.; Shkrob, I. A.; Assary, R. S.; Tung, S. O.; Silcox, B.; Duan, W. T.; Zhang, J. J.; Su, C. C.; Hu, B.; Pan, B. F.; Liao, C.; Zhang, Z. C.; Wang, W.; Curtiss, L. A.; Thompson, L. T.; Wei, X. L.; Zhang, L. Annulated Dialkoxybenzenes as Catholyte Materials for Non-Aqueous Redox Flow Batteries: Achieving High Chemical Stability through Bicyclic Substitution. *Adv. Energy Mater.* **2017**, *7*, 1701272.
(29) Wei, X. L.; Xu, W.; Huang, J. H.; Zhang, L.; Walter, E.; Lawrence, C.; Vijayakumar, M.; Henderson, W. A.; Liu, T. B.; Cosimbescu, L.; Li, B.; Sprenkle, V.; Wang, W. Radical Compatibility with Nonaqueous Electrolytes and Its Impact on an All-Organic Redox Flow Battery. *Angew. Chem., Int. Ed.* **2015**, *54*, 8684−8687.
(30) Carino, E. V.; Diesendruck, C. E.; Moore, J. S.; Curtiss, L. A.; Assary, R. S.; Brushett, F. R. BF_3-Promoted Electrochemical Properties of Quinoxaline in Propylene Carbonate. *RSC Adv.* **2015**, *5*, 18822−18831.
(31) Goulet, M.-A.; Aziz, M. J. Flow Battery Molecular Reactant Stability Determined by Symmetric Cell Cycling Methods. *J. Electrochem. Soc.* **2018**, *165*, A1466−A1477.
(32) Tong, L. C.; Goulet, M. A.; Tabor, D. P.; Kerr, E. F.; De Porcellinis, D.; Fell, E. M.; Aspuru-Guzik, A.; Gordon, R. G.; Aziz, M. J. Molecular Engineering of an Alkaline Naphthoquinone Flow Battery. *ACS Energy Lett.* **2019**, *4*, 1880.
(33) Goulet, M. A.; Tong, L. C.; Pollack, D. A.; Tabor, D. P.; Odom, S. A.; Aspuru-Guzik, A.; Kwan, E. E.; Gordon, R. G.; Aziz, M. J. Extending the Lifetime of Organic Flow Batteries Via Redox State Management. *J. Am. Chem. Soc.* **2019**, *141*, 8014−8019.
(34) Luo, J.; Hu, B.; Debruler, C.; Bi, Y.; Zhao, Y.; Yuan, B.; Hu, M.; Wu, W.; Liu, T. L. Unprecedented Capacity and Stability of Ammonium Ferrocyanide Catholyte in pH Neutral Aqueous Redox Flow Batteries. *Joule* **2019**, *3*, 149−163.
(35) Beh, E. S.; De Porcellinis, D.; Gracia, R. L.; Xia, K. T.; Gordon, R. G.; Aziz, M. J. A Neutral pH Aqueous Organic−Organometallic Redox Flow Battery with Extremely High Capacity Retention. *ACS Energy Lett.* **2017**, *2*, 639−644.
(36) Kwabi, D. G.; Lin, K.; Ji, Y.; Kerr, E. F.; Goulet, M.-A.; De Porcellinis, D.; Tabor, D. P.; Pollack, D. A.; Aspuru-Guzik, A.; Gordon, R. G.; Aziz, M. J. Alkaline Quinone Flow Battery with Long Lifetime at pH 12. *Joule* **2018**, *2*, 1894−1906.
(37) Ji, Y. L.; Goulet, M. A.; Pollack, D. A.; Kwabi, D. G.; Jin, S. Y.; De Porcellinis, D.; Kerr, E. F.; Gordon, R. G.; Aziz, M. J. A Phosphonate-Functionalized Quinone Redox Flow Battery at near-Neutral pH with Record Capacity Retention Rate. *Adv. Energy Mater.* **2019**, *9*, 1900039.
(38) Mavrodi, D. V.; Blankenfeldt, W.; Thomashow, L. S. Phenazine Compounds in Fluorescent Pseudomonas Spp. Biosynthesis and Regulation. *Annu. Rev. Phytopathol.* **2006**, *44*, 417−445.
(39) Coffield, J. E.; Mamantov, G.; Zingg, S. P.; Smith, G. P. Reduction of Aromatic-Compounds in Organic Chloroaluminate Melts. 1. Phenazine. *J. Electrochem. Soc.* **1991**, *138*, 2543−2549.
(40) Wang, R.; Okajima, T.; Kitamura, F.; Kawauchi, S.; Matsumoto, N.; Thiemann, T.; Mataka, S.; Ohsaka, T. Catalytic Reduction of O_2 by Pyrazine Derivatives. *J. Phys. Chem. A* **2004**, *108*, 1891−1899.
(41) Winsberg, J.; Stolze, C.; Muench, S.; Liedl, F.; Hager, M. D.; Schubert, U. S. Tempo/Phenazine Combi-Molecule: A Redox-Active Material for Symmetric Aqueous Redox-Flow Batteries. *ACS Energy Lett.* **2016**, *1*, 976−980.
(42) Hollas, A.; Wei, X.; Murugesan, V.; Nie, Z.; Li, B.; Reed, D.; Liu, J.; Sprenkle, V.; Wang, W. A Biomimetic High-Capacity Phenazine-Based Anolyte for Aqueous Organic Redox Flow Batteries. *Nature Energy* **2018**, *3*, 508−514.
(43) Kour, H.; Paul, S.; Singh, P. P.; Gupta, R. A Mild and Simple Method for the Synthesis of Substituted Phenazines. *Synlett* **2014**, *25*, 495−500.
(44) Iseminger, P. W.; Gregory, M.; Weakley, T. J. R.; Caple, G.; Sykes, A. G. Characterization of 3-Aminophenazin-2-Ol Isolated from the Chemical Oxidation of O-Phenylenediamine. *J. Org. Chem.* **1997**, *62*, 2643−2645.
(45) Orita, A.; Verde, M. G.; Sakai, M.; Meng, Y. S. A biomimetic redox flow battery based on flavin mononucleotide. *Nat. Commun.* **2016**, *7*, 13230.
(46) da Cunha, A. R.; Duarte, E. L.; Lamy, M. T.; Coutinho, K. Protonation/Deprotonation Process of Emodin in Aqueous Solution and pK(a) Determination: UV/Visible Spectrophotometric Titration and Quantum/Molecular Mechanics Calculations. *Chem. Phys.* **2014**, *440*, 69−79.
(47) Casida, M. E.; Jamorski, C.; Casida, K. C.; Salahub, D. R. Molecular Excitation Energies to High-Lying Bound States from Time-Dependent Density-Functional Response Theory: Characterization and Correction of the Time-Dependent Local Density Approximation Ionization Threshold. *J. Chem. Phys.* **1998**, *108*, 4439−4449.
(48) Stratmann, R. E.; Scuseria, G. E.; Frisch, M. J. An Efficient Implementation of Time-Dependent Density-Functional Theory for the Calculation of Excitation Energies of Large Molecules. *J. Chem. Phys.* **1998**, *109*, 8218−8224.
(49) Treimer, S.; Tang, A.; Johnson, D. C. A Consideration of the Application of Koutecky-Levich Plots in the Diagnoses of Charge-Transfer Mechanisms at Rotated Disk Electrodes. *Electroanalysis* **2002**, *14*, 165−171.
(50) Esswein, A. J.; Goeltz, J.; Amadeo, D. High solubility iron hexacyanides. U.S. Patent Application US15/166,176, 2014.
(51) Jin, S. J.; Jing, Y.; Kwabi, D. G.; Ji, Y. L.; Tong, L. C.; De Porcellinis, D.; Goulet, M. A.; Pollack, D. A.; Gordon, R. G.; Aziz, M. J. A Water-Miscible Quinone Flow Battery with High Volumetric Capacity and Energy Density. *ACS Energy Lett.* **2019**, *4*, 1342−1348.

https://dx.doi.org/10.1021/acsenergylett.9b02676
ACS Energy Lett. 2020, 5, 411−417